Annex 1: PRIAT Logo

Annex 2: Figures

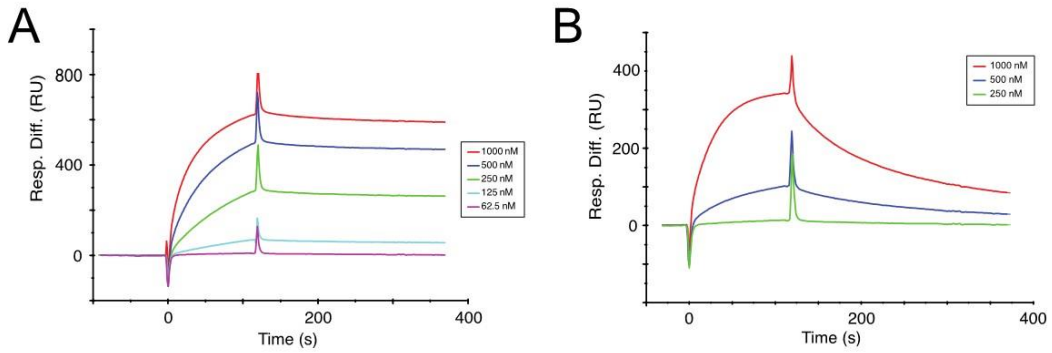

*Figure 1: Affinity measurements against human beta-2 Microglobulin via surface plasmon resonance (SPR). SPR measurements of the scFv antibody "B13" (anti-human-B2M) against human MHC-I (A; Subtype A*02:01) and against human beta-2 Microglobulin (B).*

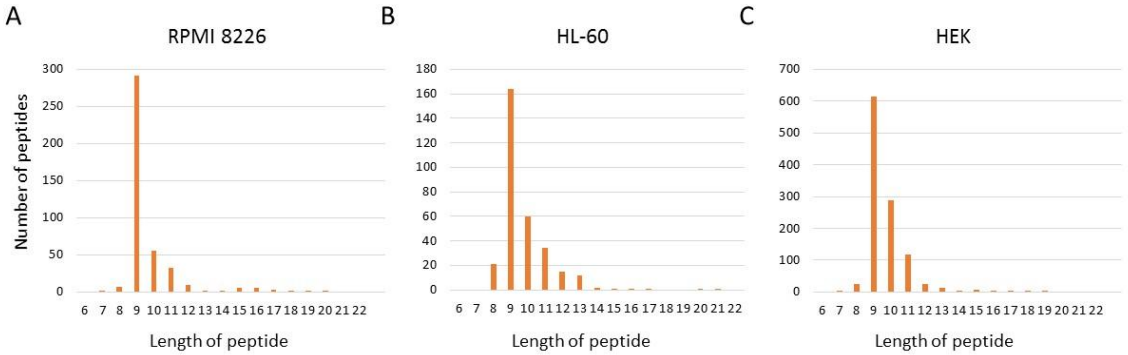

Figure 2: Length distribution of peptides identified in the analyses of (A) RPMI8226, (B) HL-60, and (C) HEK cell lines. In all cases, the majority of peptides are nine amino acids in length

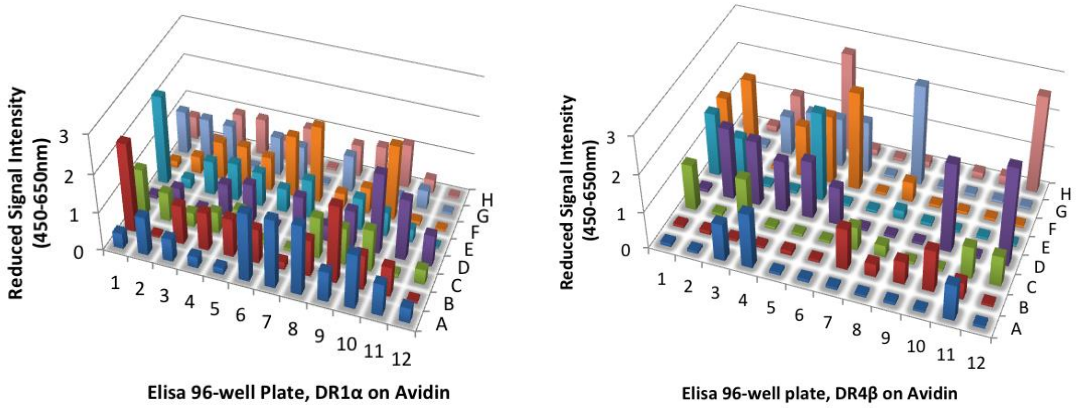

Figure 3: ELISA signals of antibody clones, derived from phage display selections against human HLA-II/CLIP complex.

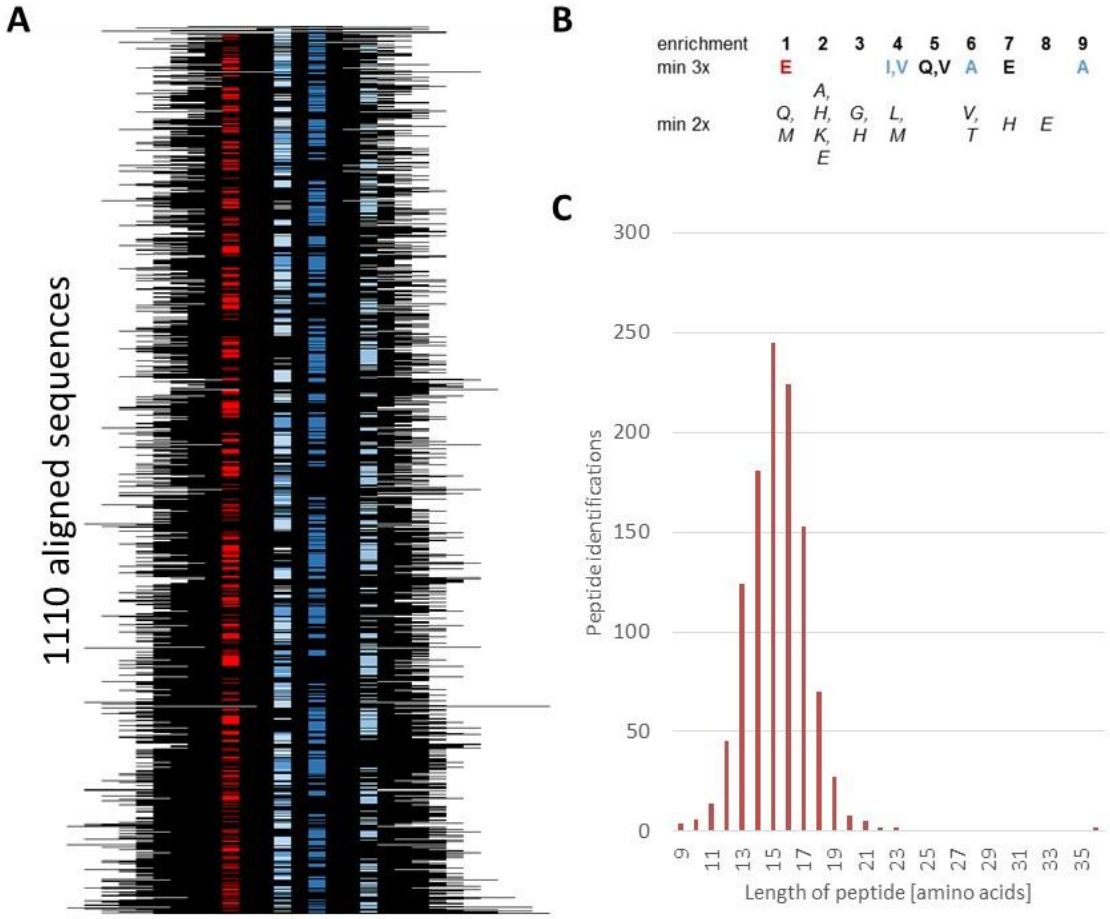

Figure 4: MHC class II eluted peptides from murine A20 lymphoma cells. A) Aligned peptide sequences are outlined in black. Certain for the binding motif central amino acids have been highlighted in color: Red: E at position 1, blue: I and V at position 4, dark blue: A at position 6, blue-gray: A at position 9. B) The binding motif as seen after alignment of the 1110 identified peptides. Amino acids enriched >3 fold over their general distribution in the proteome are displayed in bold. Amino acids enriched >2 fold are presented in italic. C) Length distribution of MHC class II peptides identified with 1% FDR in a single run starting from the lysate of 100 mio A20 lymphoma cells.

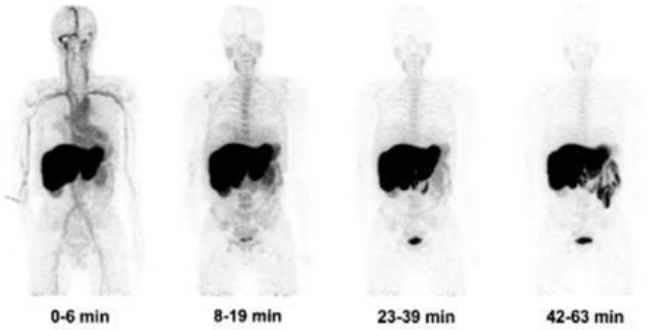

Figure 5: PET imaging of a patient with malignant mesothelioma, at various time points following administration of ^{11}C-docetaxel. The drug can be seen in liver, but also in the blood pool at early time points and in other structures (e.g., bones), but fails to preferentially localize in the neoplastic masses.

Similar observations have been reported for other cancer types and for other low molecular weight anti-cancer drugs.

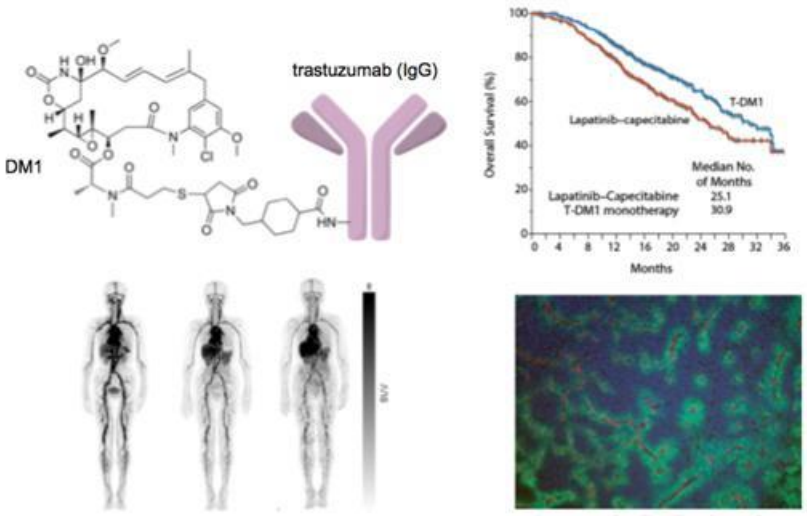

Figure 6: Top panels: schematic representation of Kadcyla™, an antibody-drug conjugate consisting of the trastuzumab antibody coupled to the potent cytotoxic drug DM1. The overall survival data that led to the approval of the drug are reported in the right panel. Bottom panels: immuno-PET findings with radiolabeled trastuzumab in a patient with breast cancer. The tumor targeting performance is far from ideal, in part due to the IgG format of the antibody. Microscopic studies of tumor sections reveal that only a subset of tumor cells is reached by trastuzumab in vivo (green), i.e. perivascular cells.

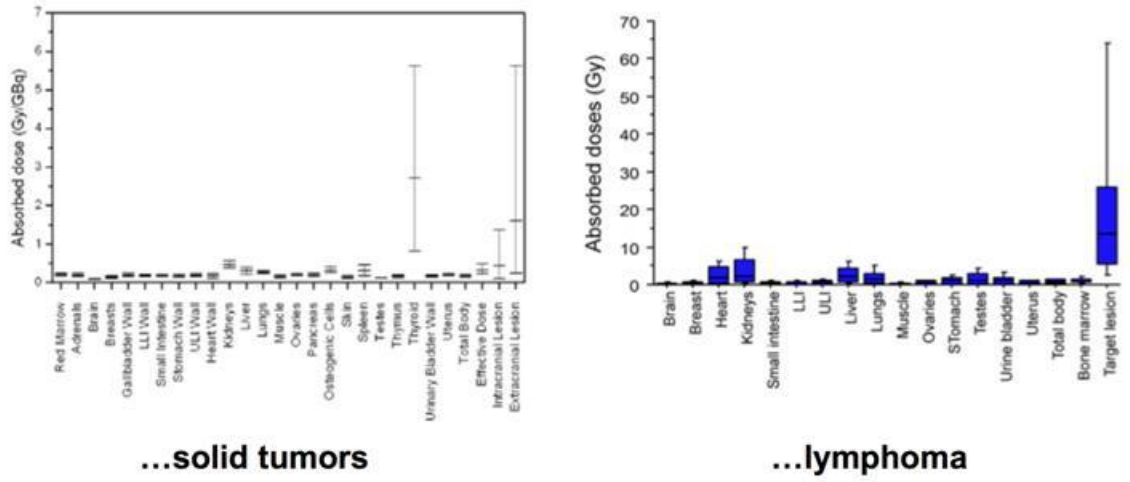

Figure 7: Absorbed doses in patients with solid tumors and with lymphomas, who received an intravenous administration of radioiodinated L19 antibody products [adapted from Poli et al. (2013) Cancer Immunol. Res., 1, 134 and from Erba et al. (2012) J. Nucl. Med., 53, 922].

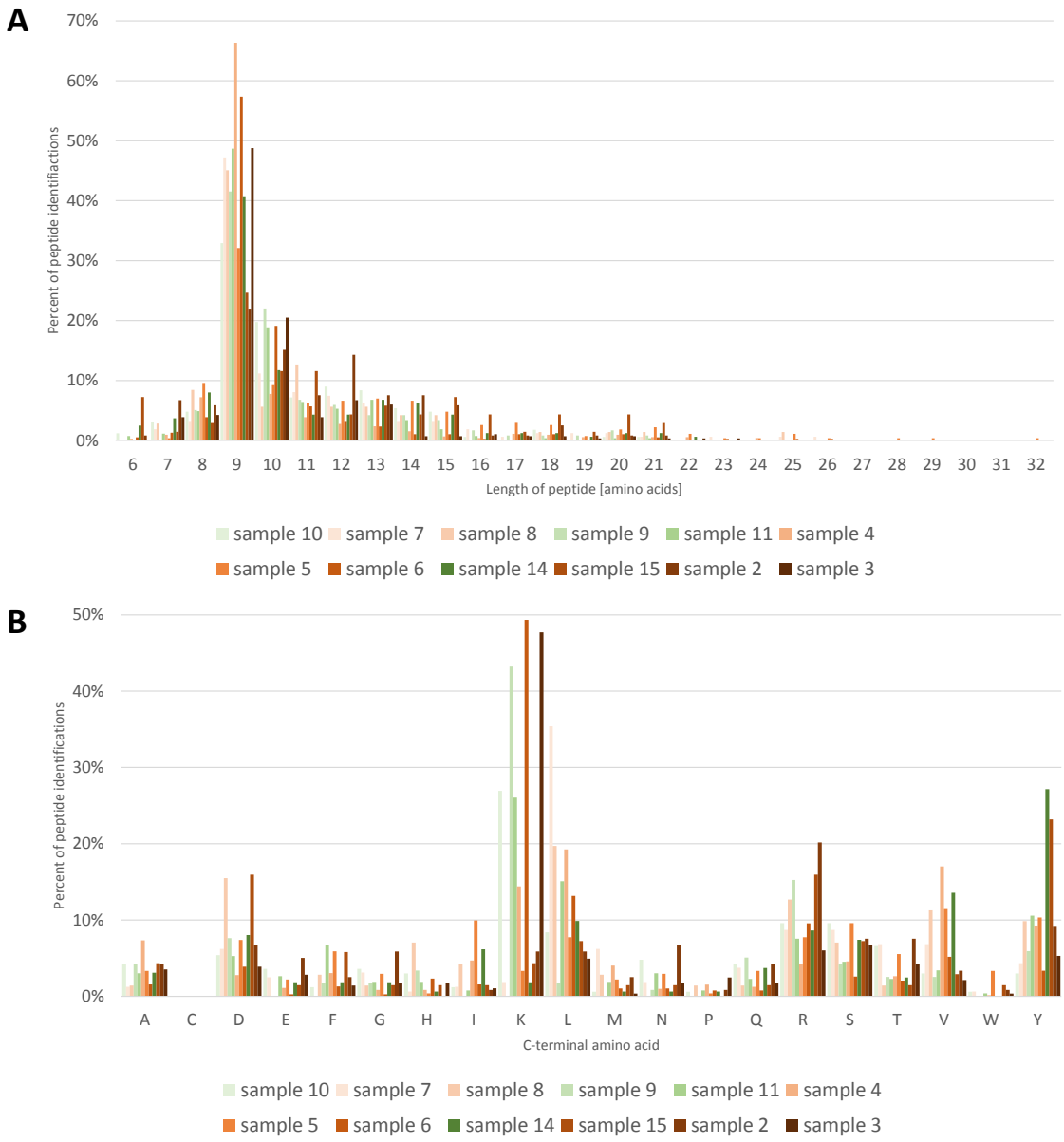

Figure 8: Characteristics of the peptides identified from melanoma patients and healthy donors. Samples are colored by their sample group: brown, cancer patients; green, healthy individuals. A) Length distribution of the identified peptides. Most peptides are nine amino acids in length. B) C-terminal amino acid. Specific patterns are visible for individual samples. Most enriched amino acids are K, L, Y, R, V, S suggesting many of the identified peptides display HLA specific anchor residues.

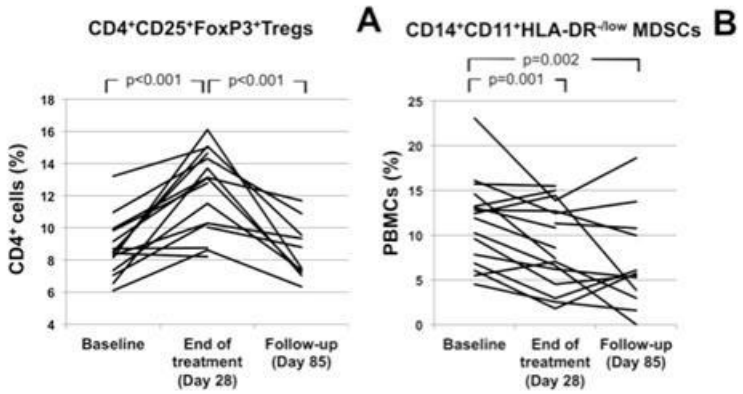

Figure 9: Systemic immune responses. (A) Frequency of CD4⁺CD25⁺Fox-P3⁺ Tregs. (B) Frequency of CD14⁺CD11b⁺HLA-DR⁻/low MDSCs.

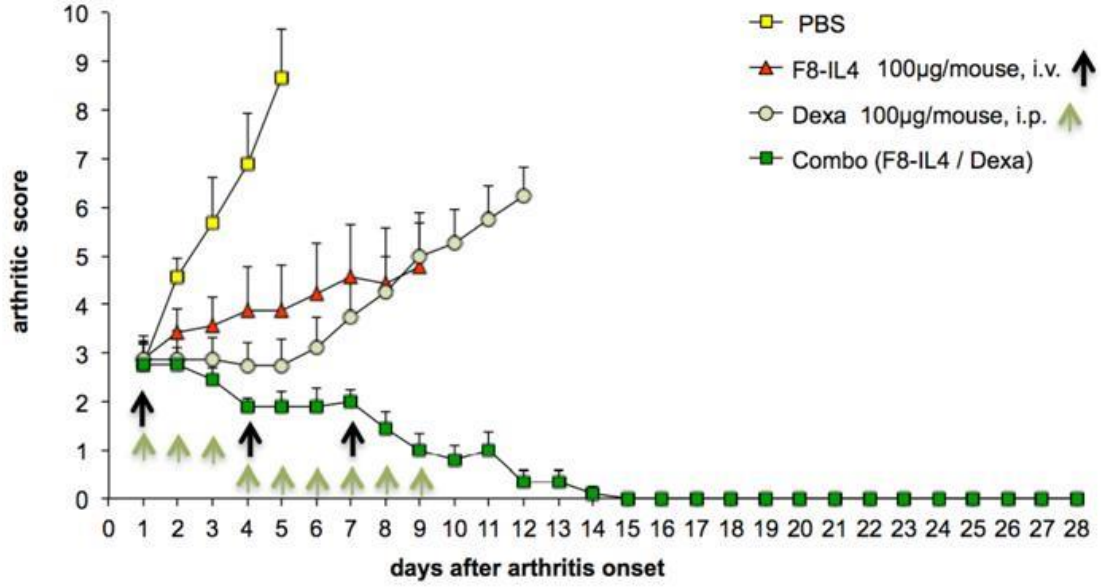

Figure 10: Therapeutic activity of F8-IL4 in the collagen-induced arthritis model. The therapeutic proteins were administered three times every 72 h (n = 7–9; SEM). The combination of F8-IL4 and daily doses of dexamethasone could cure all mice in this setting, whereas F8-IL4 or dexamethasone alone could only inhibit disease progression [Hemmerle et al. (2014) Proc. Natl. Acad. Sci. U.S.A., 111, 12008].

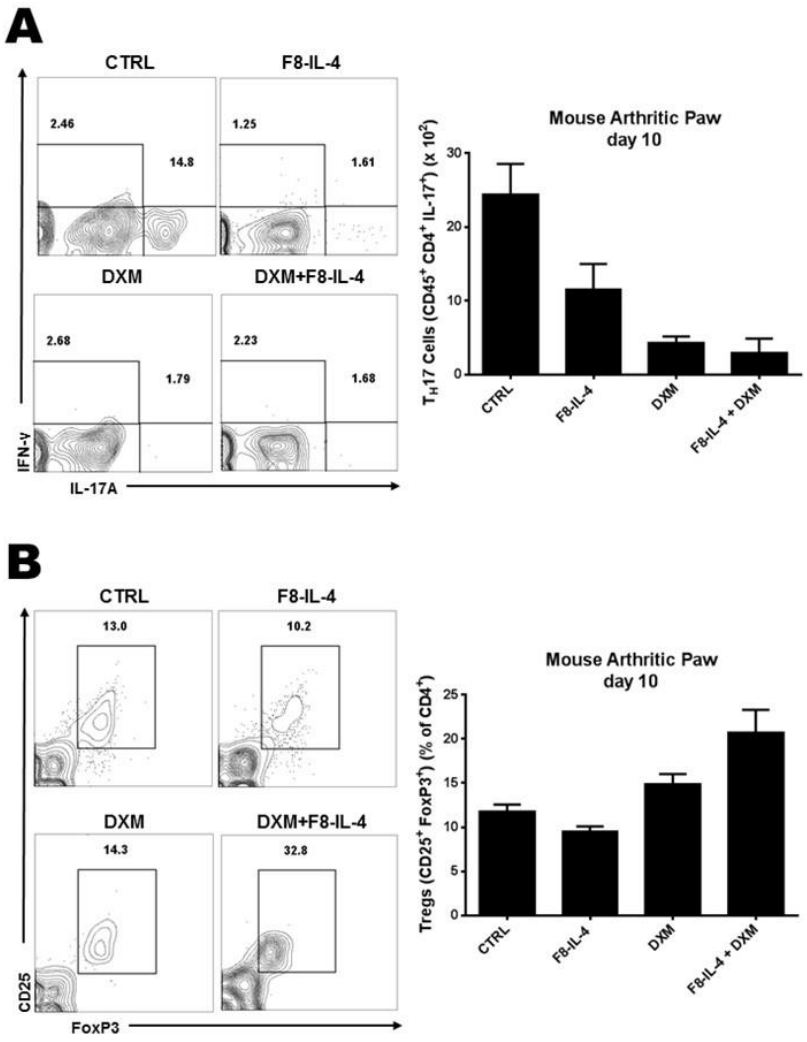

Figure 11: F8-IL-4 + DXM combination therapy leads to a significant decrease in (A) T_H17 and increase in (B) T_{reg} cells in arthritic paws of CIA mice (n = 10 per group). (C) DXM, dexamethasone.

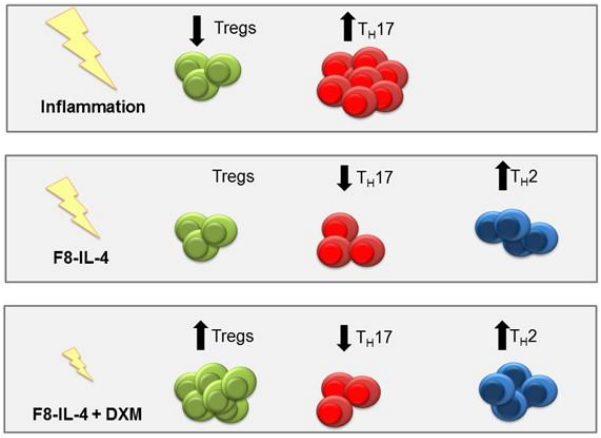

Figure 12: Proposed mechanism of action of F8-IL-4 + DXM combination therapy on immune cell balance in the joints of arthritic mice. DXM, dexamethasone.

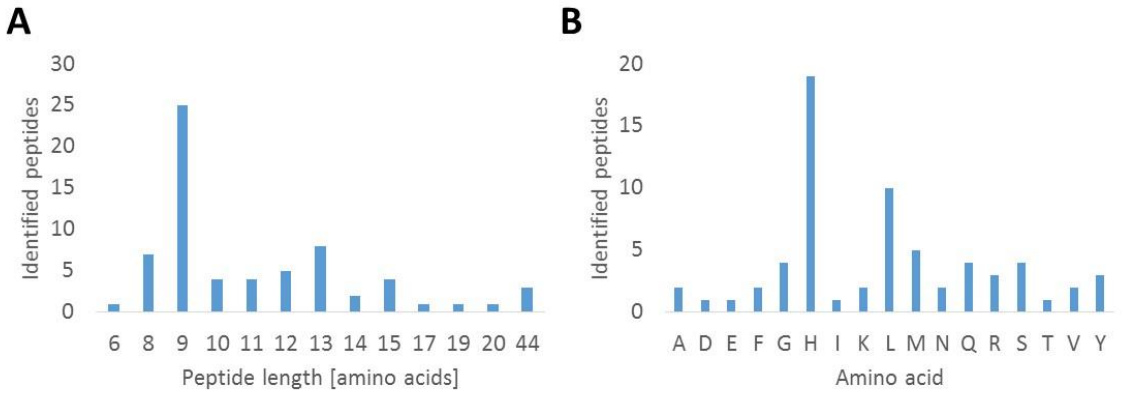

Figure 13: Characterization of peptides identified from rat sera with different grade of transplant rejection. A) Peptide length distribution demonstrating an enrichment of 9mers. B) C-terminal amino acid of identified peptides shows enrichment of peptides with c-terminal histidine and leucine.

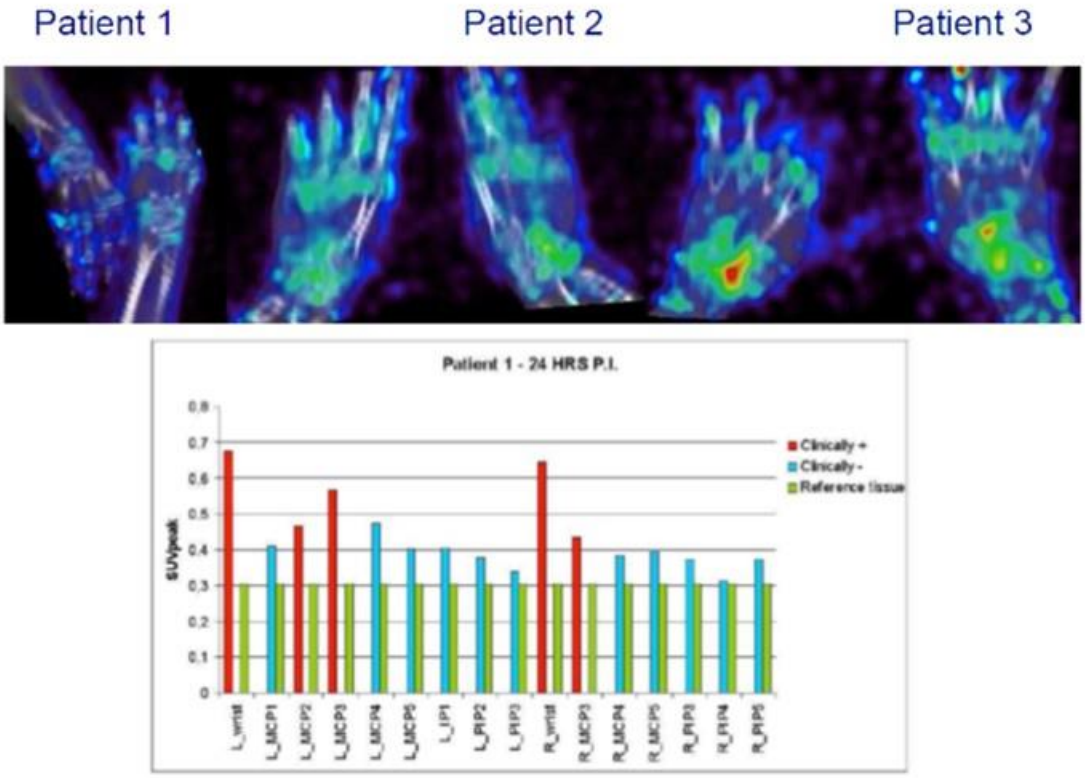

Figure 14: Top panels: ^{124}I-F8-IL10 PET image of the hands of a RA patient with clinically active disease, 24 hr p.i. Green colour represents uptake of the tracer in joints. Bottom panel: dosimetry of radiolabeled product uptake in the arthritis and non-arthritic joints of one of the studied patients.

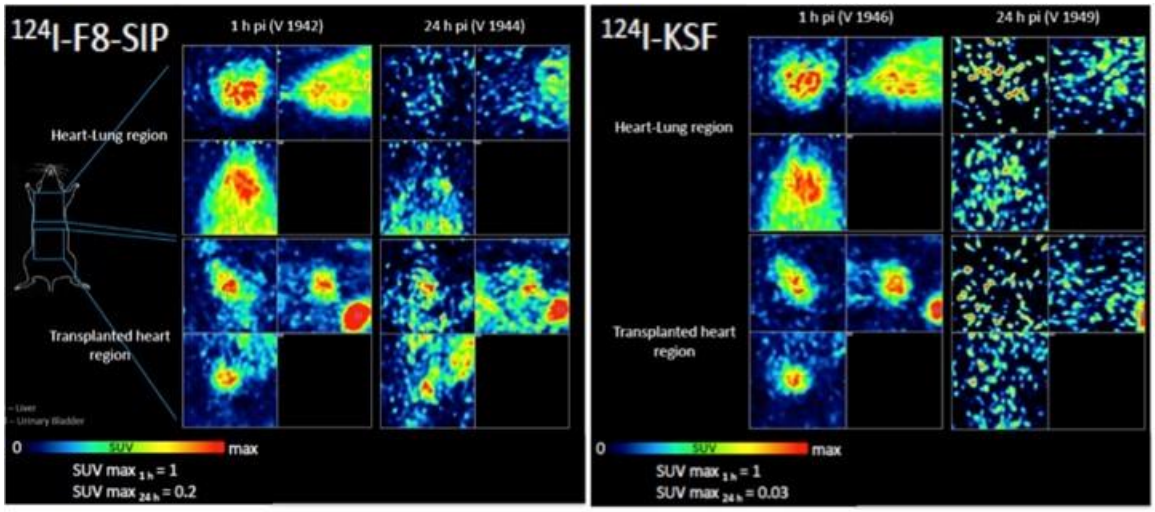

Figure 15: Immuno-PET CT imaging of rats with a heart transplant injected with ^{124}I-labeled SIP-F8 or ^{124}I-labeled SIP-KSF.

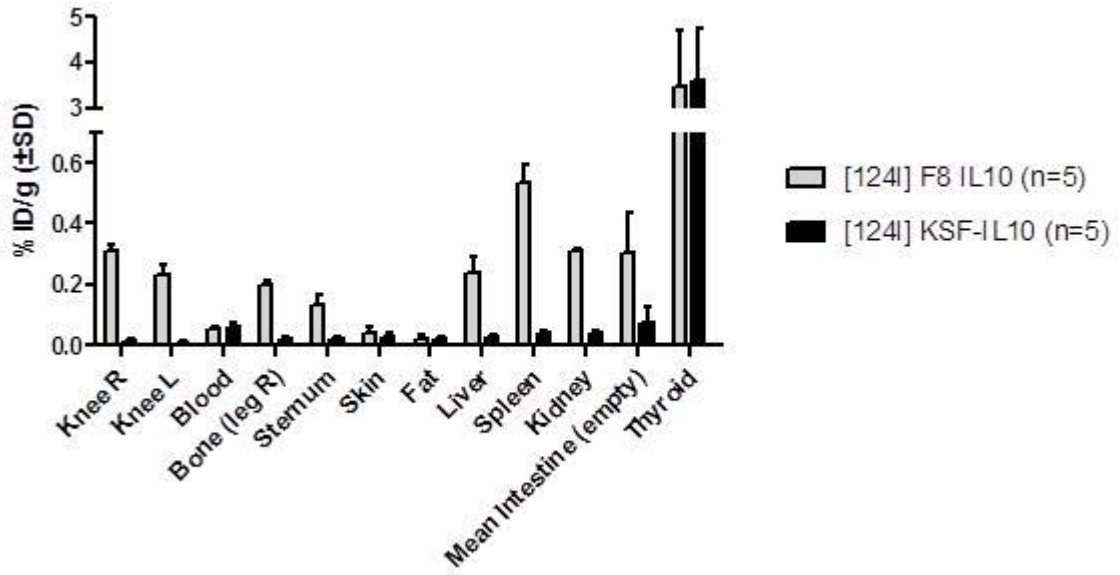

Figure 16: In vivo biodistribution of ^{124}I-F8-IL10 in arthritic rats; comparison to control agent ^{124}I-KSF-IL10.

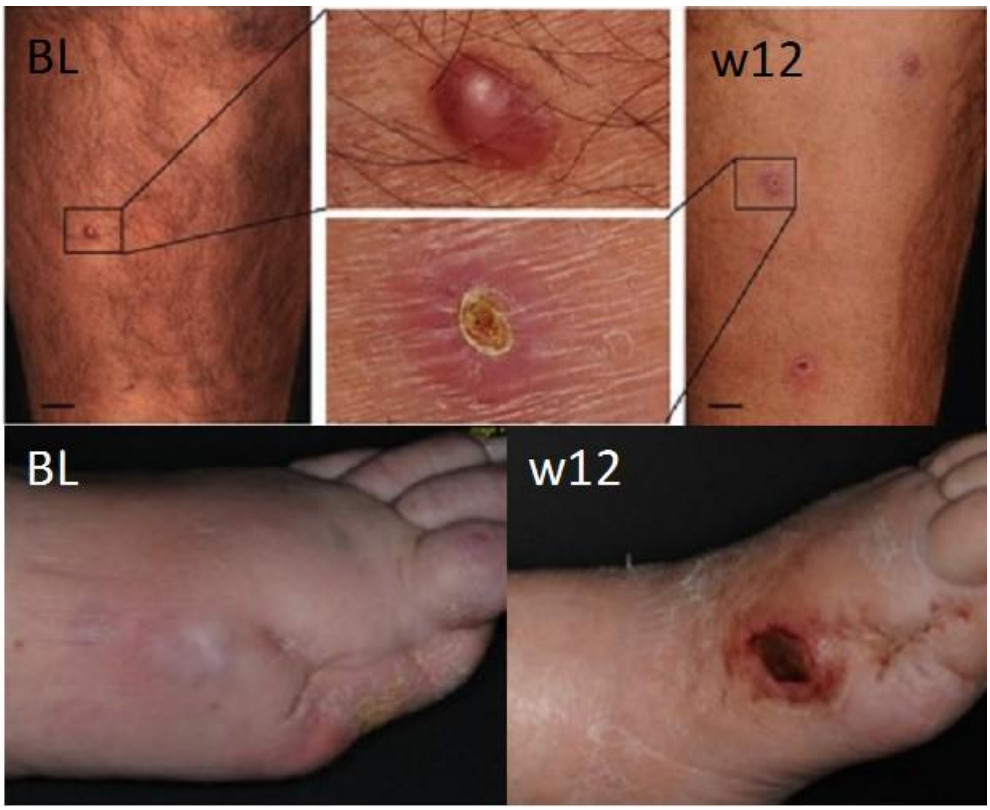

Figure 17: Clinical findings in patients who exhibited complete responses: (Upper panel) patient 27.001.L.017 at baseline and 12 weeks after first treatment; (lower panel) patient 27.002.L.019 at baseline and at week 12.

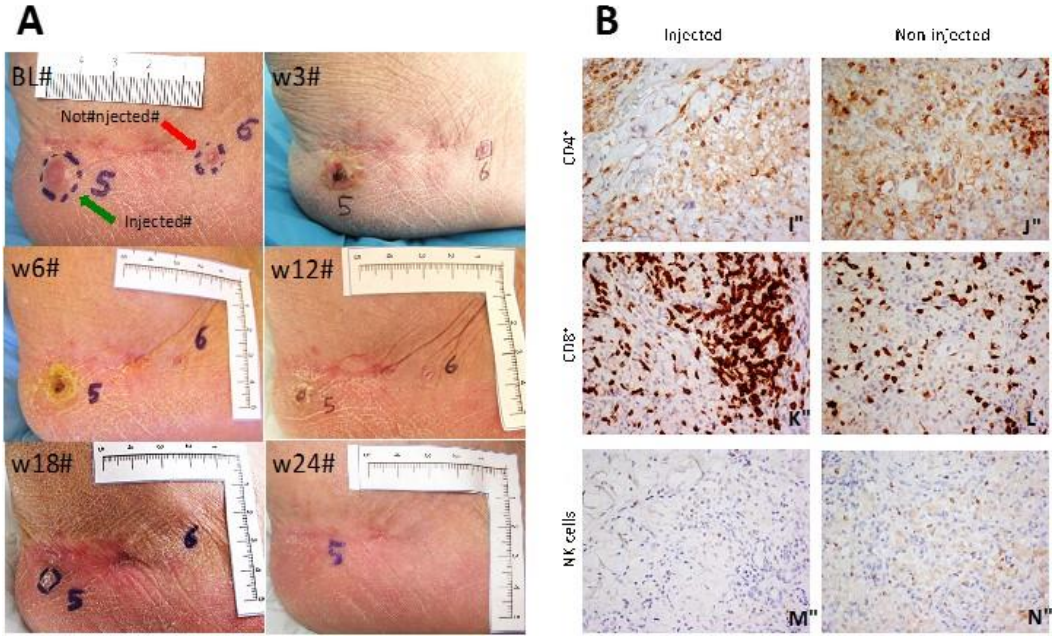

Figure 18: (A) Evidence of systemic effect on neighboring, non-injected lesions. Two cutaneous lesions were present at baseline on the right heel of patient 23.002S.004 (BL). Lesion 5 (green arrow) was injected with L19IL2 plus L19TNF, while lesion 6 (red arrow) was left uninjected. The other panels illustrate the evolution of the two lesions at the end of treatment (w3) and at week 6 (w6), week 12 (w12), week 18 (w18) and week 24 (w24) after first treatment. (B) Immunohistochemical findings in treated (panels I, K, M) vs untreated, not responding (panels J, L, N) lesions. Frequency of CD4+ T cells (panels I and J), CD8+ T cells (panels K and L) and NK cells (panel M and N) infiltration. Magnification: 200x.

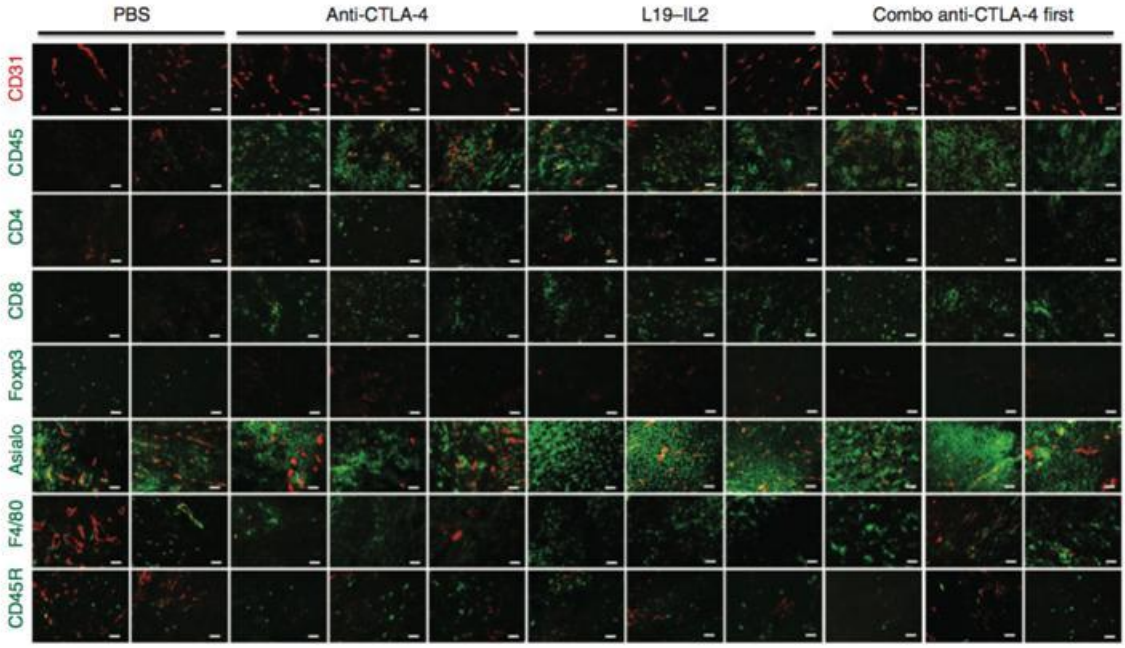

Figure 19: Immunofluorescence findings of leukocyte infiltration into tumor masses, following immunocytokine treatment in tumor-bearing mice. Red = CD31 staining. Green = staining with antibodies to antigens, indicated in the figure (vertical captions). The therapeutic antibodies used for the therapy experiments are indicated in black, on the top part of the figure.

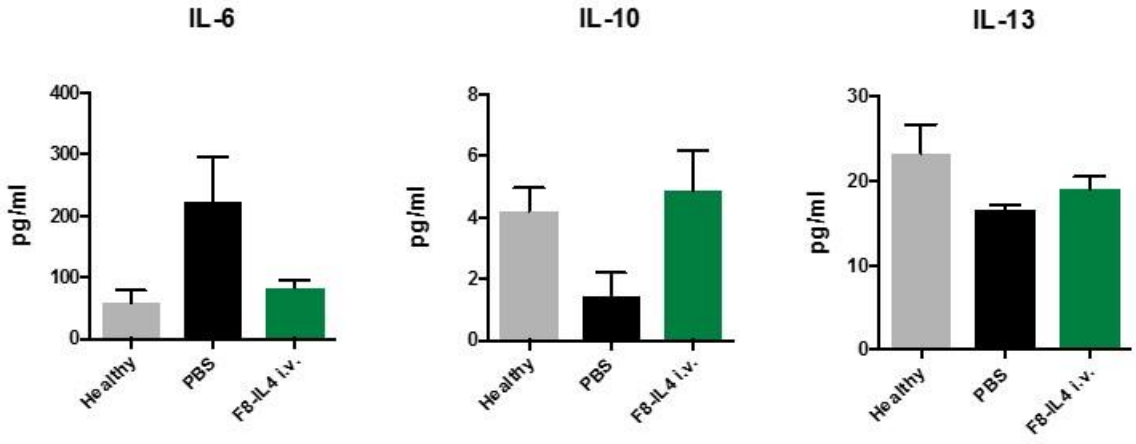

Figure 20: Serum cytokine levels in the collagen-induced arthritis model in healthy mice compared to diseased mice treated with either buffer control (PBS) or F8-IL4.

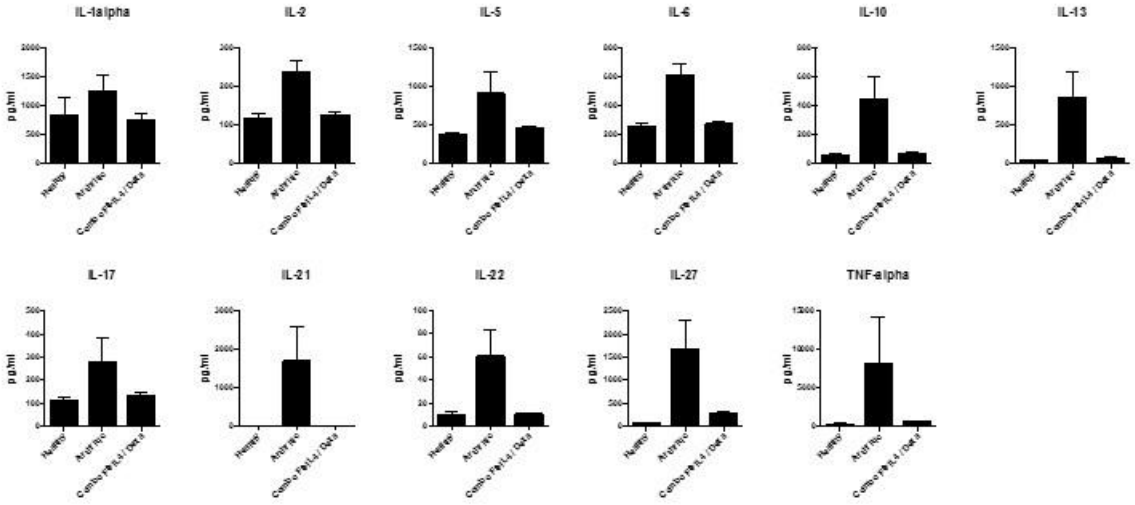

Figure 21: Analysis of cytokine levels in paws of healthy mice, mice with active arthritis and mice that are cured form established arthritis with F8-IL4 in combination with dexamethasone.

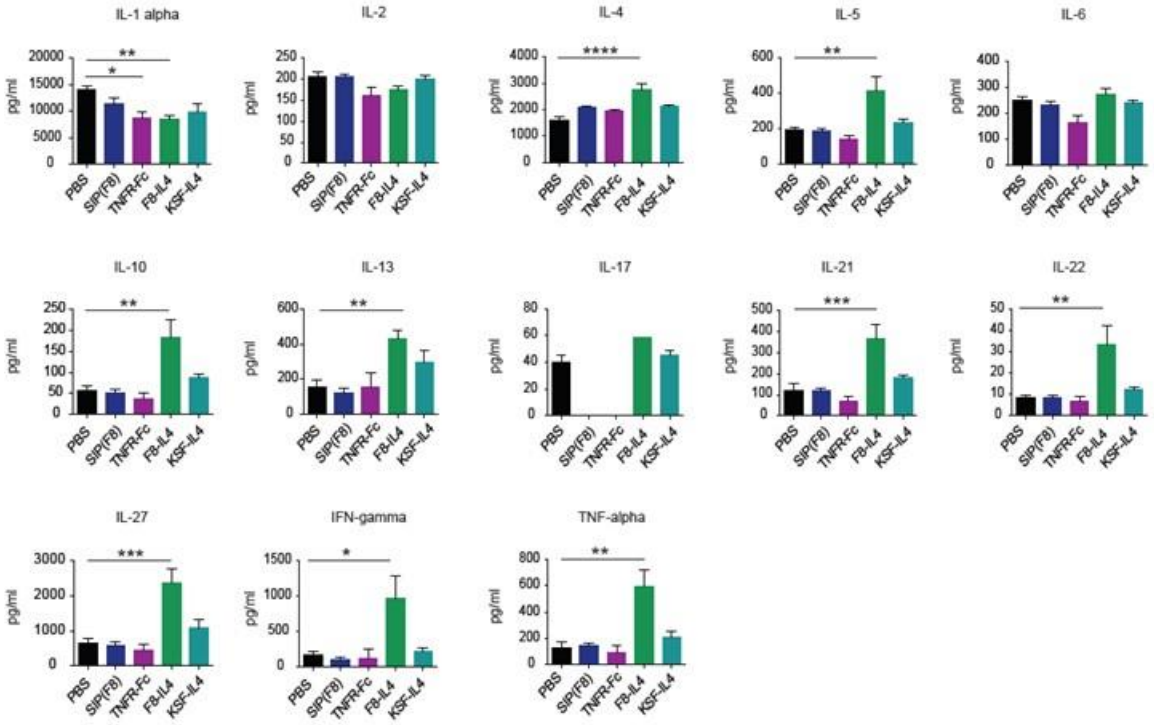

Figure 22: Analysis of cytokine levels at the site of skin inflammation of mice treated with buffer control (PBS), antibody control (F8 in small immunoprotein format SIP), fully murine TNFR-Fc, F8-IL4 and KSF-IL4 (negative control immunocytokine with no specificity in the mouse)

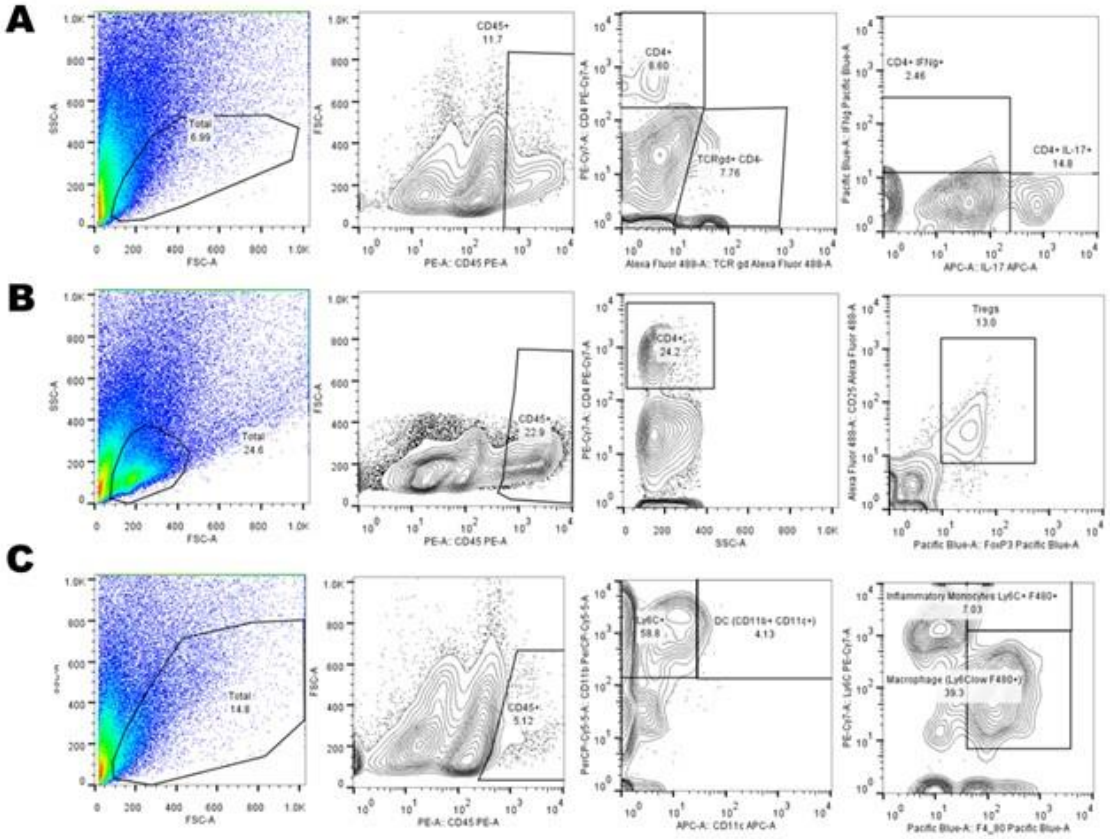

Figure 23: Examples of flow cytometric analysis of immune cell subpopulations in the paws of arthritic mice culled on day 10 post disease on-set. (A) Gating strategy for T_H17, T_H1 and TCRγδ T cells. (B) Tregs were identified as $CD45^+$ $CD4^+$ $CD25^+$ $FoxP3^+$ cells. (C) Gating strategy for cells of the myeloid lineage.

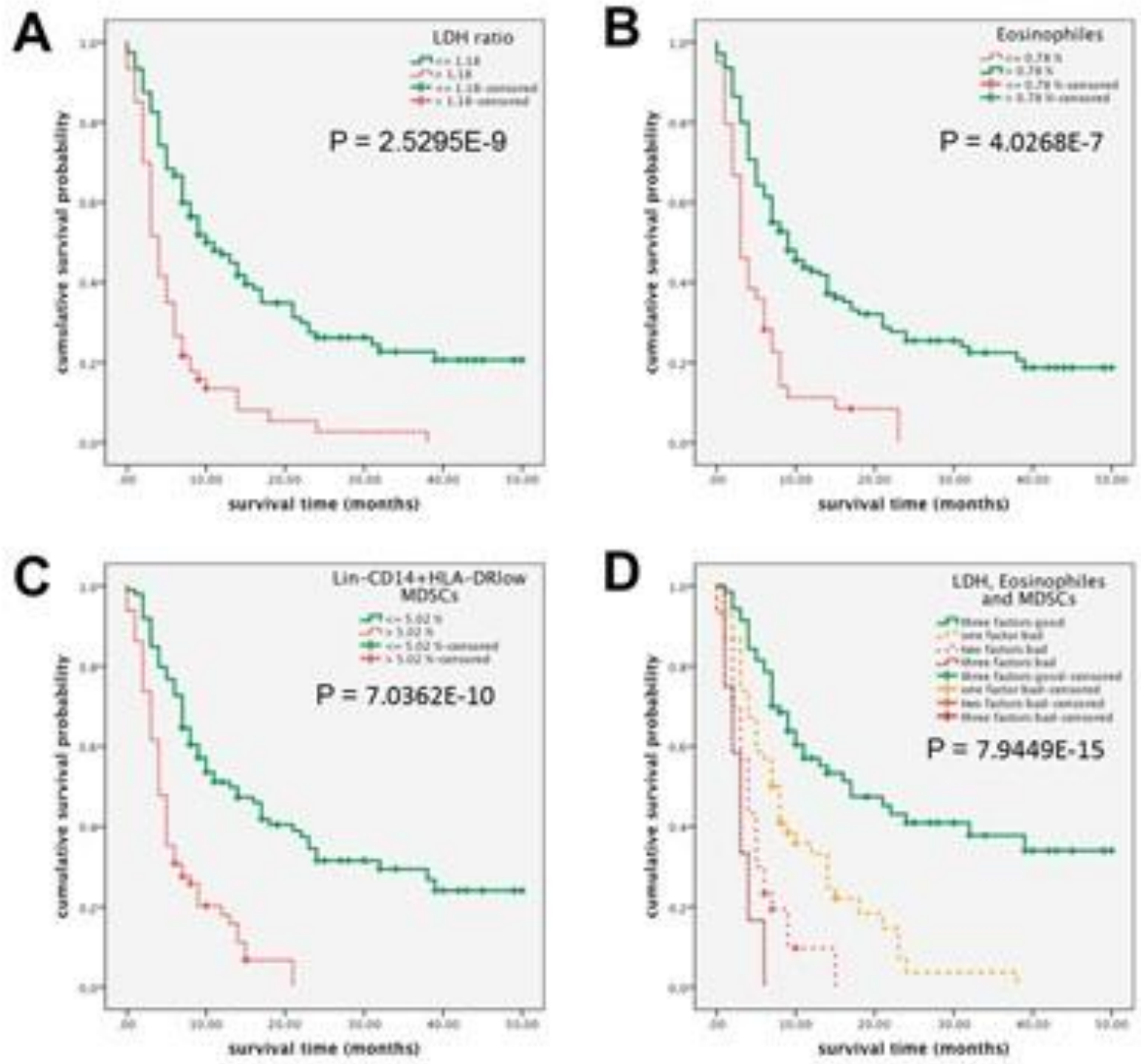

Figure 24: Survival according to Kaplan Maier for confirmed independent predictive biomarkers LDH-ratio (A), the relative eosinophil count (B) and Lin-CD14+HLA-DRlow myeloid-derived suppressor cells (C). The independent effect is demonstrated by grouping patients according to the number out of those three factors pointing towards unfavorable survival (D).

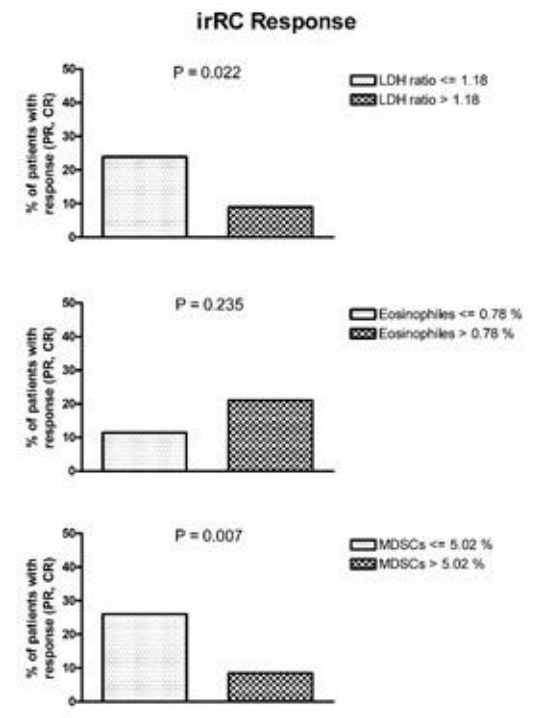

Figure 25: Response rate (sum of complete and partial best overall response) according to irRC for LDH-ratio (upper part), the relative eosinophil count (middle) and Lin-CD14+HLA-DRlow myeloid-derived suppressor cells (lower part).

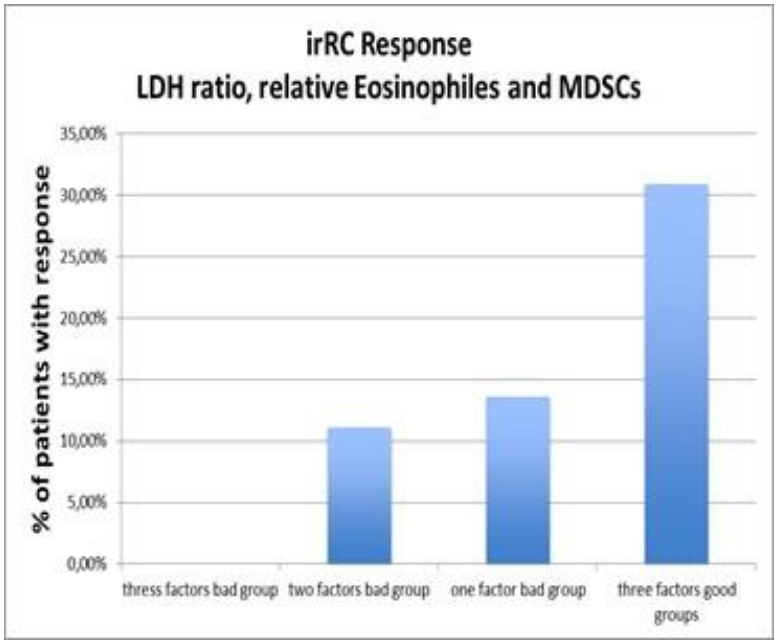

Figure 26: Response rate according to irRC for combinations of LDH-ratio, the relative eosinophil count and Lin-CD14+HLA-DRlow myeloid-derived suppressor cells.

Figure 27: Kick-off meeting with all PRIAT Partners in October 2012.

Figure 28: Mid-term meeting of the PRIAT consortium in 2013.

Figure 29: Final Project meeting with all PRIAT Partners and invited guests for the international symposium.

Figure 30: Visit of Philogen's GMP manufacturing site and joint scientific seminars on targeting with antibodies and HLA peptidomics.

Annex 3: Tables

Table 1: Details of the melanoma patient sera received from Tübingen.

Sample number	Run order	Patient ID	Serum volume	Nr. of aliquots	HLA typing	Stage	Tumor burden	Timepoint
1	n/a	Tumor01	5-10 ml	5	A2+	stage IV	none	
2	10	Tumor02pre	5-10 ml	3	A2+	stage IV	low	before Ipilimumab
3	12	Tumor03	5-10 ml	5	A2+	stage IV	medium	during Ipilimumab
4	8	Tumor04	5-10 ml	5	A2+	stage IV	high	during Ipilimumab
5	7	Tumor05	5-10 ml	9	A2+	stage IV	high	before Ipilimumab
6	6	Tumor06	5-10 ml	4	A2+	stage IV	high	
7	4	Tumor07	5-10 ml	4	A2+	stage III	none	
8	3	Tumor08	5-10 ml	1	A2+	stage III	none	
9	1	Healthy01	5-10 ml	1	A2+	healthy		
10	2	Healthy02	5-10 ml	1	A2+	healthy		
11	5	Healthy03	5-10 ml	1	A2+	healthy		
12	n/a	Healthy04	5-10 ml	1	A2+	healthy		
13	n/a	Healthy05	5-10 ml	1	A2+	healthy		
14	9	Healthy06	5-10 ml	1	A2+	healthy		
15	11	Tumor02post	5-10 ml	1	A2+	stage IV CR	low	after Ipilimumab free of disease

Table 2: Selection of the peptides identified from 5ml of CIA mouse serum. Peptides are derived from membrane proteins, intracellular proteins, and collagens.

Peptide sequence	Protein Name	Accession	Gene
QQPREEETDSKSFDEMEQSLL	ATP-binding cassette sub-family A member 5	Q8K448	Abca5
SPTPTEGDQDDRSYKQCRTSSPS	Actin-binding LIM protein 2	D3Z0Y4	Ablim2
FVHPWDMQMDGRMAKYWLPWLVGMP SETTMAICSMIMGG	2-amino-3-carboxymuconate-6-semialdehyde decarboxylase	Q8R519	Acmsd
GIHETTFNSIM	Actin, cytoplasmic 2	P63260	Actg1
VSTGDCPFIVCMTYAFHTPDKLCFILDLMN GGDMHYHLSQ	Beta-adrenergic receptor kinase 2	Q3UYH7	Adrbk2
GQSSGSSNFGGFPTASHSSFQPQTTG	Arf-GAP domain and FG repeat-containing protein 1	Q8K2K6	Agfg1
RGPIKTKQFAPIH	ATP synthase subunit beta, mitochondrial	P56480	Atp5b
ERGPIKTKQFAPIH	ATP synthase subunit beta, mitochondrial	P56480	Atp5b
GPIKTKQFAPIH	ATP synthase subunit beta, mitochondrial	P56480	Atp5b
TTAYFLYQQQGR	H-2 class II histocompatibility antigen gamma chain	P04441	Cd74
TGFPGAAGRVGPPGP	Collagen alpha-1(I) chain	P11087	Col1a1
SGNAGPPGPPGPVGKEGGKGPRG	Collagen alpha-1(I) chain	P11087	Col1a1
TGPAGRPGEVGPPGPPGP	Collagen alpha-1(I) chain	P11087	Col1a1
TGSPGSPGPDGKTGPPGP	Collagen alpha-1(I) chain	P11087	Col1a1
TGPIGPPGPAGAPGDKGEA	Collagen alpha-1(I) chain	P11087	Col1a1
TAGEPGKAGERGLPGPPGAVGP	Collagen alpha-1(I) chain	P11087	Col1a1
TGFPGAAGRTGPPGP	Collagen alpha-2(I) chain	Q01149	Col1a2
SRGPSGAPGPDGNKGEAGAVGAPGSA GASGPGG	Collagen alpha-2(I) chain	Q01149	Col1a2
SGPAGPRGSPGERGEVGP	Collagen alpha-2(I) chain	Q01149	Col1a2
HGPPGKDGTSGHPGPIGPPGPRG	Collagen alpha-1(III) chain	P08121	Col3a1
QGPVGPPGFTGPPGPPGP	Collagen alpha-1(IV) chain	P02463	Col4a1
TNPPLIQEKPAKTS	Eukaryotic translation initiation factor 4 gamma 2	Q62448	Eif4g2
HEYVADVEKHSSQTD	Hematopoietic lineage cell-specific protein	P49710	Hcls1
YQIREKEFPKARG	Lysosome-associated membrane glycoprotein 3	Q7TST5	Lamp3
LPSAPGCIAPGP	Nuclear receptor subfamily 4 group A member 3	Q9QZB6	Nr4a3
TSTDTPIYSQVAPR	Tyrosine-protein phosphatase non-receptor type 18	Q61152	Ptpn18
DITNTDTFARAK	Ras-related protein Rab-5C	P35278	Rab5c
YDITNTDTFARAK	Ras-related protein Rab-5C	P35278	Rab5c
HGSGKEETSIEAKIRAKE	Regulator of G-protein signaling 18	Q99PG4	Rgs18
TVVFPGGDKGKIAS	Trem-like transcript 1 protein	Q8K558	Treml1
NGGGGGVSARSVAG	Protein Tsc22d2	E9Q7M2	Tsc22d2
KTSAAPGGVPLQPQDL	Cytochrome b-c1 complex subunit 2, mitochondrial	Q9DB77	Uqcrc2

Table 3: Antibody-Panels for staining of immune cell subsets and subsequent flowcytometry.

T cell panel	Treg Panel	MDSC Panel	γ/δ T cell Panel
CD3	CD3	CD3	CD45RA
CD4	CD4	CD4	CD16
CD8	CD8	CD11b	CD28
CD19	CD25	CD14	vd2
CD27	CD45RA	CD15	CD4
CD28	CD103	CD16	vd1
CD45RA	CD127	CD19	CD27
PD-1	FoxP3	CD40	CD8
ICOS	Ki67	CD56	CD3
CCR7	EOMES	HLA-DR	pan γ/δ
OX40		IL4Ra	

Table 4: Overview over associations between biomarker and overall survival.

Factor	Dichotomized based on the median value from cohort 1		Dichotomized based on the median value from cohort 2	Dichotomized based on the median value from cohort 2			optimized cut-offs in cohort 2	optimized cut-offs in cohort 2	
	Cohort 1		Cohort 2	Cohort 3			Cohort 2	Cohort 3	
	N=25		N=85	N=99			N=85	N=99	
	p-Value		p-Value	p-Value			p-Value	p-Value	
LDH-ratio	0,117		0,083	0,000			0,000	0,000	Confirmed
Gender	0,809		0,768	0,243					
Age	0,579		0,753	0,982			0,382	0,268	
M-category (no consideration of LDH)	0,063		0,001	0,429	not conf.				
Leucocytes blood count	0,728		0,009	0,833	not conf.		0,000	0,137	not conf.
Abs lymphocytes differential blood count	0,867		0,450	0,579			0,027	0,870	not conf.
Rel lymphocytes differential blood count	0,348		0,041	0,273	not conf.		0,000	0,181	not conf.
Abs eosinophils differential blood count	0,596		0,177	0,005			0,138	0,005	
Rel eosinophils differential blood count	0,047		0,071	0,000			0,002	0,000	Confirmed
Abs monocytes differential blood count	0,068		0,000	0,341	not conf.		0,000	0,549	not conf.
Rel monocytes differential blood count	0,776		0,251	0,923			0,004	0,948	not conf.
CD4pos_CD8pos FACS	0,451		0,021	0,723	not conf.		0,003	0,517	not conf.
CD25posFoxP3pos_CD4pos FACS	0,833		0,797	0,075			0,198	0,136	
CD4posCD127lowCD25posFoxP3pos_CD4pos FACS	na		0,963	0,294			0,042	0,089	Confirmed
CD4posCD127lowCD25posFoxP3posCD45RAnegKi67pos_CD4pos FACS	na		0,001	0,012	Confirmed		0,001	0,021	Confirmed
CD4posCD127lowCD25posFoxP3posKi67negCD45RAdim_CD4pos FACS	na		0,834	0,200			0,329	0,084	
Ki67pos_CD4pos FACS	na		0,709	0,081			0,090	0,882	
CD8pos_CD8pos FACS	0,415		0,008	0,595	not conf.		0,007	0,595	not conf.
Ki67pos_CD8pos FACS			0,738	0,139			0,063	0,229	
CD14pos_allcells FACS	0,068		0,009	0,974	not conf.		0,000	0,943	not conf.
CD14posHLADRlow_allcells FACS			0,000	0,083	not conf.		0,000	0,010	Confirmed
LinnegCD14posHLADRlow_allcells FACS	0,006		0,000	0,134	not conf.		0,000	0,002	Confirmed

Table 5: Univariate analysis for three confirmed independent predictive markers

Factor	n	n	Deaths	%	% dead	Median survival (months)	p-value	1-year survival rate (95% CI)		2-year survival rate (95% CI)		3-year survival rate (95% CI)	
LDH ratio													
≤ 1,18	180	120	83	66,7%	69,2%	11	2,53E-09	46,5%	[37,3%; 55,6%]	27,3%	[18,6%; 35,9%]	22,7%	[14,1%; 31,3%]
> 1,18		60	56	33,3%	93,3%	4		12,1%	[3,7%; 20,5%]	4,8%	[0,0%; 11,0%]	2,4%	[0,0%; 7,0%]
missing	4												
Relative Eosinophiles													
≤ 0,78 %	179	39	37	21,8%	94,9%	3	4,03E-07	11,7%	[1,5%; 21,8%]	1,7%	[0,0%; 6,2%]		
> 0,78 %		140	99	78,2%	70,7%	9		41,9%	[33,5%; 50,3%]	26,8%	[18,8%; 34,8%]	21,6%	[13,7%; 29,5%]
missing	5												
Lin-CD14+HLA-DRlow MDSCs													
≤ 5,02 %	164	99	64	60,4%	64,6%	13	7,04E-10	49,7%	[39,6%; 59,9%]	34,0%	[23,9%; 44,1%]	28,5%	[18,3%; 38,7%]
> 5,02 %		65	58	39,6%	89,2%	4		18,4%	[8,8%; 28,0%]	2,3%	[0,0%; 6,7%]		
missing	20												